NeuroImage 75 (2013) 58–67

Contents lists available at SciVerse ScienceDirect

NeuroImage

journal homepage: www.elsevier.com/locate/ynimg

Prediction of individual subject's age across the human lifespan using diffusion tensor imaging: A machine learning approach

Benson Mwangi [a,*], Khader M. Hasan [b], Jair C. Soares [a]

[a] UT Center of Excellence on Mood Disorders, Department of Psychiatry and Behavioral Sciences, UT Houston Medical School, Houston, TX, USA
[b] The University of Texas Health Science Center at Houston, Department of Diagnostic & Interventional Imaging, Houston, TX, USA

ARTICLE INFO

Article history:
Accepted 27 February 2013
Available online 14 March 2013

Keywords:
Diffusion tensor imaging
Cerebral maturation
Cerebral ageing
Neuroimaging
Multivariate
Machine learning
Relevance vector regression

ABSTRACT

Diffusion tensor imaging has the potential to be used as a neuroimaging marker of natural ageing and assist in elucidating trajectories of cerebral maturation and ageing. In this study, we applied a multivariate technique relevance vector regression (RVR) to predict individual subject's age using whole brain fractional anisotropy (FA), mean diffusivity (MD), axial diffusivity (AD) and radial diffusivity (RD) from a cohort of 188 subjects aged 4–85 years. High prediction *accuracy* as derived from Pearson correlation coefficient of actual versus predicted age (FA — $r = 0.870$ $p < 0.0001$; MD — $r = 0.896$ $p < 0.0001$; AD — $r = 0.895$ $p < 0.0001$; RD — $r = 0.899$ $p < 0.0001$) was achieved. Cerebral white-matter regions that contributed to these predictions include; corpus callosum, cingulum bundles, posterior longitudinal fasciculus and the cerebral peduncle. A post-hoc analysis of these regions showed that FA follows a nonlinear rational-quadratic trajectory across the lifespan peaking at approximately 21.8 years. The MD, RD and AD volumes were particularly useful for making predictions using grey matter cerebral regions. These results suggest that diffusion tensor imaging measurements can reliably predict individual subject's age and demonstrate that FA cerebral maturation and ageing patterns follow a non-linear trajectory with a noteworthy peaking age. These data will contribute to the understanding of neurobiology of cerebral maturation and ageing. Most notably, from a neuropsychiatric perspective our results may allow differentiation of cerebral changes that may occur due to natural maturation and ageing, and those due to developmental or neuropsychiatric disorders.

Introduction

Post-mortem studies have previously shown that the human brain undergoes several changes during maturation and ageing. These changes include, myelin level changes (Benes et al., 1994), synaptic density variations (Huttenlocher, 1979; Huttenlocher and de Courten, 1987) and Schwann cell subunit density changes (Kanda et al., 1991). Recently though, magnetic resonance imaging (MRI) techniques such as diffusion tensor imaging (DTI) have allowed characterization of anatomical tissue in vivo. This has led to increased interest in applying DTI measurements in lifespan cerebral maturation and ageing studies as demonstrated in these detailed reviews (Cascio et al., 2007; Gunning-Dixon et al., 2009; Johansen-Berg and Behrens, 2009; Moseley, 2002; Sullivan and Pfefferbaum, 2006).

Several DTI microstructural measurements have proved to be particularly important in this endeavour and below we briefly explore these measurements. First, fractional anisotropy (FA) is used to quantify tissue water diffusion directionality or anisotropy in vivo (Basser and Pierpaoli, 1996). A higher FA value (maximum = 1, minimum = 0) represents diffusion occurring along one direction but largely restricted in all other directions (Johansen-Berg and Behrens, 2009). Higher FA values are often associated with highly myelinated white-matter tracts and vice versa (Hasan et al., 2008; Klingberg et al., 1999; Kochunov et al., 2012). Numerous studies have used FA as a proxy measure of myelin levels with success (Abe et al., 2002; Barnea-Goraly et al., 2005; Eluvathingal et al., 2007; Grieve et al., 2007; Hasan et al., 2008; Head et al., 2004; Hsu et al., 2010; Kennedy and Raz, 2009; Kochunov et al., 2012; Lebel et al., 2008, 2012; Ota et al., 2006; Pfefferbaum et al., 2000; Salat et al., 2005a; Schmithorst et al., 2002; Westlye et al., 2010). In a nutshell, these studies point to two consistent themes. First, FA increases consistently during healthy childhood and adolescence in a majority of white matter tracts. Second, FA decreases consistently with ageing. These results have also been confirmed by white matter volumetric studies showing that white matter tissue undergoes

* Corresponding author at: Department of Psychiatry and Behavioral Sciences, University of Texas Health Science Center at Houston, 1941 East Road, Houston, TX 77054, USA.
E-mail address: Benson.Irungu@uth.tmc.edu (B. Mwangi).

1053-8119/$ – see front matter © 2013 Elsevier Inc. All rights reserved.
http://dx.doi.org/10.1016/j.neuroimage.2013.02.055

accelerated volumetric changes during early and late life with a plateau in early and middle adulthood (Westlye et al., 2010). Specifically, age related FA decline has been reported in anterior cingulum bundles, frontal gyrus, cerebral peduncle and corpus callosum (Brown et al., 2012; Malykhin et al., 2011; Pfefferbaum et al., 2005; Salat et al., 2005a; Sullivan and Pfefferbaum, 2006; Virta et al., 1999). Notably, FA decline is statistically comparable in both male and female and linear from about 20 years onwards (Malykhin et al., 2011; Ota et al., 2006; Pfefferbaum and Sullivan, 2003; Sullivan and Pfefferbaum, 2006; Virta et al., 1999).

Other DTI measurements which offer complementary information not available with FA include radial diffusivity (RD), mean diffusivity (MD) and axial diffusivity (AD). Since tissue water molecular anisotropy and diffusivity are not only specific to white-matter tissue (Q. Wang et al., 2010), we envisaged that these additional DTI-derived metrics may be predictive of individual subject's age as well to help in elucidating the cerebral maturation and ageing process in both grey and white matter tissues. Correspondingly, several studies have recently applied MD, AD and RD to study diffusivity in both white and grey matter tissues with success (Benedetti et al., 2006; Kumar et al., 2012; Ota et al., 2006; Song et al., 2002, 2003; Stadlbauer et al., 2008b; Q. Wang et al., 2010). In particular, studies comparing healthy young and older adults conclude that AD and MD in grey matter tissue increase considerably with ageing (Abe et al., 2008; Bhagat and Beaulieu, 2004; Camara et al., 2007; Hasan, 2010; Hasan and Frye, 2011; Kochunov et al., 2010; Liu et al., 2012; Pfefferbaum et al., 2010; Stadlbauer et al., 2008a).

However, despite gaining significant insights into cerebral maturation and ageing using these DTI measurements, many studies preceding this report have mainly used pre-defined regions-of-interest (ROIs) and to some extent whole-brain data with *univariate* data analysis techniques (Johansen-Berg and Behrens, 2009; Whitcher et al., 2007). In this study, we adopted a multivariate machine-learning technique with whole-brain FA, MD, AD and RD to predict individual subject's age. There are two notable benefits in adopting this approach. First, the ability to accurately and efficiently decode a continuous variable (e.g. age) from neuroimaging scans (Haynes and Rees, 2006; Johnston et al., 2012; Mwangi et al., 2012a, 2012b). This is achieved by separating training and test data using a *cross-validation* process. Second, the possibility to select anatomical regions relevant to the decoding process, a step commonly known as feature subset selection (FSS) in machine learning. This process takes into account interactions of full spatial anatomical patterns without necessarily making any a-priori assumptions (Ziegler et al., 2012). This is particularly important as it has been reported that cerebral ageing is a 'global' process affecting major white-matter tracts simultaneously (Penke et al., 2010).

Multivariate machine learning regression models have recently been used to decode continuous targets (e.g. age, clinical scores) from neuroimaging scans with success (Brown et al., 2012; Cherubini et al., 2009; Dosenbach et al., 2010; Formisano et al., 2008; Franke et al., 2010; Kohannim et al., 2012; Mwangi et al., 2012a; Stonnington et al., 2010; Y. Wang et al., 2010).

In this study, we applied the relevance vector regression (RVR) algorithm (Tipping, 2001) to predict individual subject's age using whole brain FA, MD, RD and AD volumes. Specific benefits of using RVR over other equivalent algorithms such as support vector regression (SVR) (Smola and Scholkopf, 2004) should be noted. First, RVR selects relatively few features (sparse) resulting to efficiency in making predictions (Tipping, 2001). Second, RVR estimates model 'nuisance' or regularisation parameters automatically (Bishop, 2006; Tipping, 2001). In this study, anatomical voxels (features) relevant in making accurate predictions were selected using a multivariate recursive feature elimination method (Guyon and Elisseeff, 2003). A post-hoc analysis of these 'relevant' anatomical features was used to evaluate cross-sectional cerebral maturation and ageing trajectories. A major objective was to elucidate whether these maturation and ageing trajectories follow linear or non-linear paths.

Materials and methods

Subjects and DTI acquisition protocol

Raw diffusion tensor scans were acquired from the International Neuroimaging Data Sharing Initiative (INDI) online database (http://fcon_1000.projects.nitrc.org/indi/pro/nki.html). Additional variables included subjects' age and a battery of clinical assessment scores. This sample was provided by the Nathan Kline Institute (NKI, NY, USA) as part of the '*original NKI-Rockland sample*'. All necessary approvals and procedures for human subject studies were followed as required by NKI. DTI images were acquired using a 3.0 T Siemens Trio scanner with a spin echo — EPI factor = 128, TE/TR = 91/10,000 ms, FOV = 256 mm, spatial resolution = 2.0 × 2.0 × 2.0 mm, 64 diffusion encoding gradients, b-value = 1000 s/mm^2 and 12 non-diffusion volumes. Further details about the study image acquisition protocol are available on the INDI website as above. These data have been made available to all researchers around the world for the purpose of discovery science and potentially, for replication of results in different laboratories.

DTI pre-processing

DTI images were pre-processed using the FSL software package Version 4.1.9 (Smith, 2002; Smith et al., 2006). In-house MATLAB routines were used to batch FSL pre-processing procedure as follows. 1) Head motion and eddy current correction. 2) Calculation and fitting of a diffusion tensor in every voxel (Smith et al., 2006). This step resulted into 'per subject' FA, MD, AD and RD image volumes. 3) Skull and non-brain tissue removal using FSL's brain extraction tool (BET). 4) Image volumes were spatially normalized into a standard template (FMRIB58_FA) by employing a non-linear registration routine (FNIRT) in FSL (Smith et al., 2006). This template is a high-resolution average of fifty eight DTI volumes from healthy male and female subjects aged between 20 and 50 years. FNIRT (Smith et al., 2006) is a non-linear volume alignment process with *intermediate* degrees of freedom which does not change the nature of the images during registration by keeping the white matter structural topology intact (Smith et al., 2006). In this study, FNIRT was implemented by a Matlab (The Mathworks, Inc.) batch execution of the '*tbss_2_reg*' routine in FSL (Smith et al., 2006).

FA voxels with FA < 0.3 were removed from subsequent analyses to avoid partial volume effects as recommended in previous studies (Chiang et al., 2009; Smith et al., 2006). A total of 207 subjects' DTI volumes with age ranging 4–85 years were acquired from the INDI database as above. Nineteen subjects' DTI volumes were discarded from subsequent analyses after artefacts were identified during visual inspection. As a result, DTI volumes of 188 healthy subjects (110 males, 78 females) with age ranging 4–85 years and mean/SD(34.9 ± 20.07) were used in subsequent analyses. A distribution histogram of subjects included in this study is given in Fig. 1. A detailed table of subjects' INDI database identifiers, corresponding age, gender and handedness is provided in the Supplementary materials (Table 2).

Machine learning

In this study, we assumed a machine learning problem with N number of training examples (subjects) represented as $\{X_i, t_i\}_{i=1}^{N}$. X_i stands for input data (e.g. subjects' FA volumes) and t_i corresponds to continuous targets (e.g. subjects' age). Our objective was to train a predictive model able to reliably estimate a target t (age) given an 'unseen' or novel sample X (e.g. FA volume). This

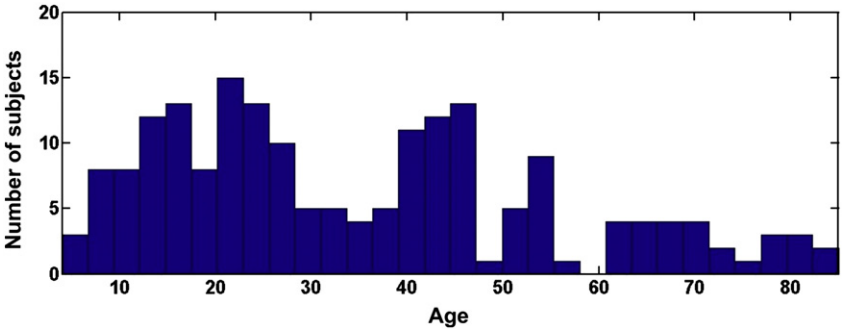

Fig. 1. A histogram of 188 subjects included in the study.

input-target pair of X_i and t_i respectively can be represented using a generalised linear model (GLM) as;

$$t_i = \sum_{i=1}^{N} \omega_i K(x, x_i) + c + \varepsilon_i \quad (1)$$

where x and x_i represent testing and training data respectively (e.g. FA volumes). $K(x_1 x_2) = \exp\left(\frac{x_1 - x_2^2}{2\sigma^2}\right)$ is a Gaussian radial basis kernel function (RBF) which is used to calculate similarities between training samples and σ is a user defined *kernel width parameter* which controls how the similarities are calculated. This parameter was estimated using a non-biassed cross-validation procedure using training data only. $W = (\omega_1, \omega_2, \ldots \omega_N)^T$ is a *weighting* vector estimated during model training. As a result, each subject data is represented by a single *weighting factor* (ω) with 'many' of them set to zero and subjects with non-zero weighting factors are used for making predictions and are referred to as *relevance vectors*. c is a model bias parameter whose value is estimated during model training, ε_i represents system's measurement noise, and t_i is our desired prediction target value (e.g. age). Consequently, the goal of training a predictive regression model here was to estimate the model's *weighting factors* and their corresponding training subject data (relevance vectors). This combination was used for making predictions on novel or 'unseen' subjects' data. A detailed description of RVR with rigorous mathematical detail on how to estimate weighting factors and corresponding samples is given in Appendix A. RVR was implemented using in house custom software based on Tipping's Relevance Vector Machines (RVMs) MATLAB (The Mathworks, Inc.) toolbox (Tipping, 2001). Leave-one-out cross-validation (LOOCV) (Lachenbruch and Mickey, 1968) was used to train and test the RVR model and a general overview of this process is further described in Fig. 2.

Multivariate feature subset selection

A DTI volume (e.g. FA or MD) from an individual subject contains (>100,000) non-zero voxels. In contrast, our training data sample size (number of subjects), at every iteration was only 187 subjects (1 subject left-out for testing). As a result, the number of voxels (features) greatly exceeded the sample size. This is a common problem in machine learning known as the *curse of dimensionality* or *small-n-large-p* and may lead to a predictive model 'overfitting' (Guyon and Elisseeff, 2003). This indicates, the model has a marked risk of being unable to generalise from *novel* or 'unseen' subjects' data.

To circumvent this problem, recursive feature elimination (RFE) (Guyon and Elisseeff, 2003; Guyon et al., 2002), a multivariate feature subset selection technique was used to select relevant voxels effectively discarding redundant voxel plus noise. This was implemented using a 10-fold cross-validation of the training data. As a result, at each of the 10-iterations (9-fold-training, 1-fold-testing), a RVR model with a non-linear radial-basis function kernel was trained and a *sensitivity map* (Kjems et al., 2002; LaConte et al., 2005; Rasmussen et al., 2011) was extracted. Left out testing dataset (1-fold) was used to select the best RBF *kernel width parameter*. Mathematical details on how to extract *sensitivity maps* from RBF trained models are given in Appendix B and elsewhere (Kjems et al., 2002; LaConte et al., 2005; Rasmussen et al., 2011). Essentially, a *sensitivity map* indicates the relevance of voxels or features to the trained model with low ranking voxels having small *sensitivity values* and vice versa. *Sensitivity maps* from the 10-iterations were averaged and a 2% of the lowest ranking voxels were removed and this was repeated whilst simultaneously evaluating the model's mean absolute error (MAE). This process was iteratively repeated until all features (voxels) in the training set were removed. Finally, voxels resulting to large MAEs (non-relevant anatomical features) were removed from both training data and the testing subject's data. The remaining voxels (relevant voxels) were used to train and test the final model. We note that RVR calculations were performed separately for FA, MD, RD and AD volumes. RFE was implemented in house using MATLAB (The Mathworks, Inc.). Fig. 3 shows evolution of RFE iterations whilst removing 2% of the lowest ranking voxels in a single LOOCV iteration. As the model was trained and tested using a LOOCV process, a *consensus sensitivity map* was generated by selecting voxels that were 'relevant' for making predictions in all LOOCV iterations. This was the case for FA, MD, RD and AD and shown in Fig. 5.

Table 1
Model prediction errors of young versus old subjects.

DTI measurement	Age group	MAE (years)	Standard deviation of residuals
FA	Young (<30.5)	6.77	5.47
	Old (>30.5)	9.64	7.72
RD	Young (<30.5)	5.38	4.23
	Old (>30.5)	8.40	6.24
MD	Young (<30.5)	5.86	4.58
	Old (>30.5)	8.52	6.33
AD	Young (<30.5)	5.17	4.30
	Old (>30.5)	9.08	6.20

Table 2
Model prediction errors of male versus female subjects.

DTI measurement	Gender group	MAE (years)	Standard deviation of residuals
FA	Male	8.18	6.32
	Female	8.24	7.52
RD	Male	6.80	5.27
	Female	7.0	5.90
MD	Male	7.06	5.61
	Female	7.36	5.77
AD	Male	6.80	5.28
	Female	7.57	6.19

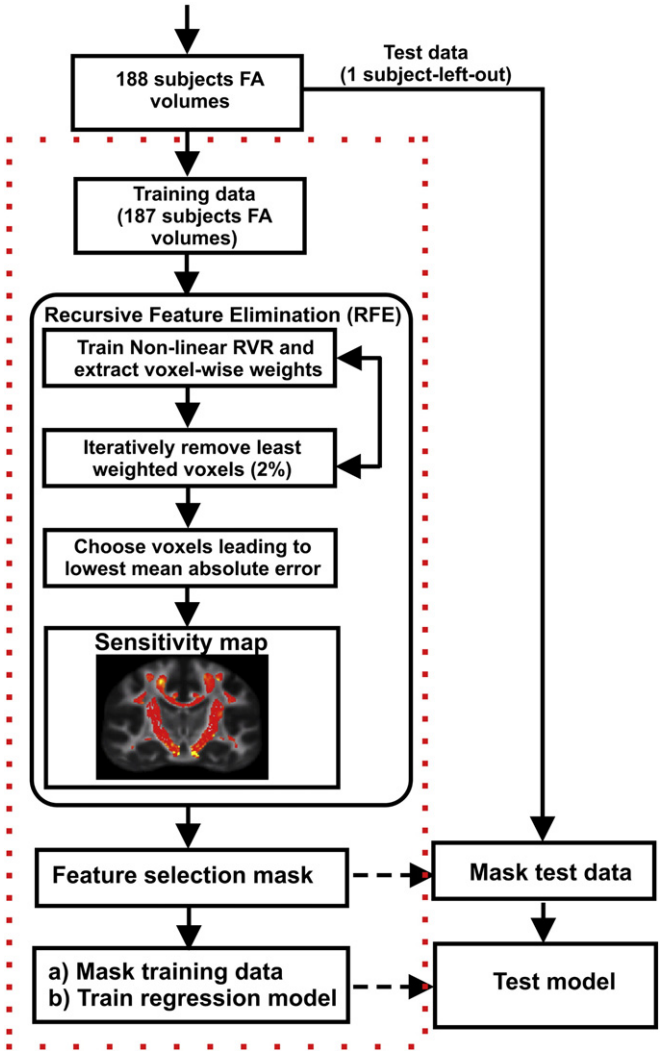

Fig. 2. Flow diagram showing the leave-one-out cross-validation process. Data was split into training (187 subjects) and testing (1 subject) and this was repeated for188 iterations until all subjects were left-out once. Relevant features were selected using training data only.

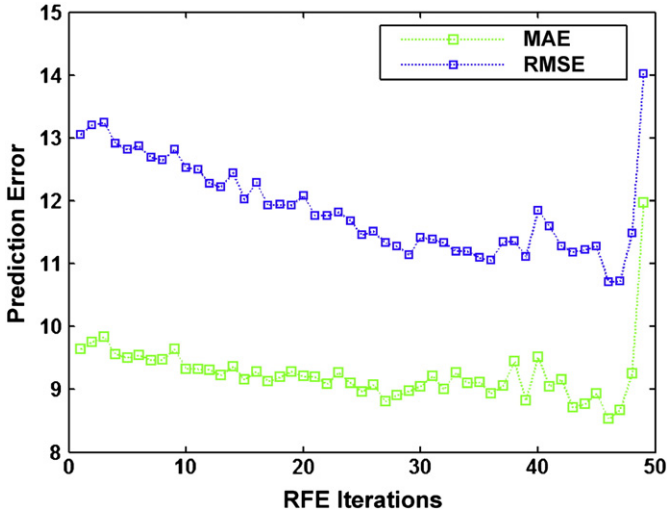

Fig. 3. MAE and RMSE curves showing the evolution of a recursive feature elimination process. 2% of features are removed at every iteration until the feature set is empty. In this case, the mean absolute and root mean square errors dropped to the lowest after 46 iterations. In the first iteration (all features present) MAE = 9.6459 and after 46 iterations MAE = 8.52. Non-relevant voxels (1st iteration to 46th iteration) were removed from both training and testing data before model training. This curve depicts only one iteration of a LOOCV process.

Model prediction evaluation

The model's 'accuracy' in predicting age from DTI scans of subjects not included during the training stage was evaluated using several statistical measures. First, Pearson correlation coefficient (r) between actual and predicted age was used to test the null hypothesis of no significant correlation. Accompanying p-values are also reported. Second, the mean absolute error (MAE) was used to measure the average magnitude of errors between actual and model predicted age. Third, root mean square error (RMSE) was used to quantify the squared difference between actual and model predicted age. RMSE is particularly useful at quantifying large errors (Mayer and Butler, 1993). Both MAE and RMSE can range from $0 - \infty$ and lower values indicate the model's ability to make predictions with high *accuracy*. Finally, the coefficient of determination r^2 was used to calculate the proportion of the variance of the predicted age which is predictable from actual age. Notably, higher r and r^2 values (maximum = 1) are indicative of a highly *accurate* regression model.

Post-hoc analysis of relevant anatomical regions

In each subject, relevant anatomical features selected through the multivariate feature selection process were averaged. These average values and corresponding subjects' actual age were fit into different polynomial functions (linear, quadratic, cubic, rational-quadratic and rational-cubic) and the function with the best goodness-of-fit chosen. Goodness-of-fit was evaluated using both graphical and numerical measures as shown in Table 3 and Fig. 6. In FA, the best-fit curve was used to calculate an approximate cerebral maturation peaking age by estimating the curve's turning point (maxima) where the curve's first derivative equalled to zero. Curve fitting was performed using in house Matlab software and Matlab's (The Mathworks, Inc.) curve fitting toolbox. More details on goodness-of-fit measures and polynomial curves are given in the Supplementary material. Average MD, RD and AD values from relevant anatomical regions were also evaluated against subjects' age and also reported in the Supplementary material.

Results

Fig. 4 summarizes RVR age prediction results from the four DTI measurements (FA, MD, AD and RD) in whole-brain white and grey matter. Overall, RD was the best in predicting age ($r = 0.899$, $p < 0.0001$). Predictions from all four DTI measurements were significant ($p < 0.0001$). Younger subjects (less than median age of 30.5 years) were predicted more accurately than older subjects (more than median age) as shown in Table 1.

Table 3
FA curve fitting goodness-of-fit statistics. The rational-quadratic function was the 'best-fit' meaning small SEE, small RMSE, large R-square and adjusted R-square.

Polynomial model	Sum of squares due to errors	Root mean squared error	R-square	Adjusted R-square
Linear	0.1086	0.024	0.28	0.28
Quadratic	0.09512	0.023	0.37	0.36
Cubic	0.09216	0.022	0.39	0.38
Rational-quadratic (quadratic/linear)	0.0824	0.02116	0.453	0.444
Rational-cubic (cubic/linear)	0.0828	0.02127	0.451	0.439

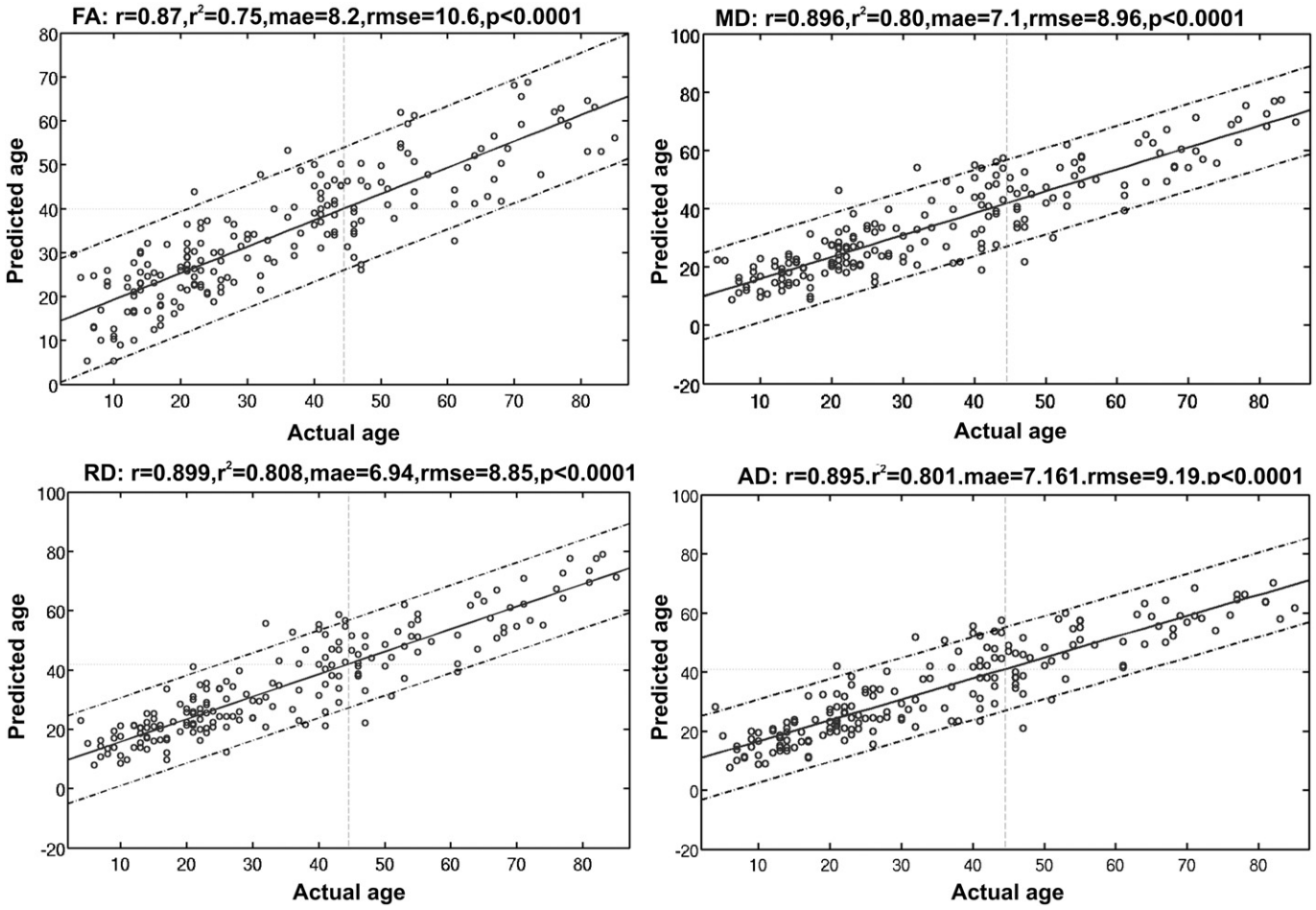

Fig. 4. FA, MD, RD and AD age prediction scatter plots depicting actual vs RVR predicted age.

Interestingly, whilst the model was exposed to whole-brain DTI volumes in MD, RD and AD the model selected grey-matter cerebral patterns as the most relevant for making predictions.

Fig. 5 shows *consensus* sensitivity maps for FA, RD, MD and AD respectively. Regions are weighted by order of importance as indicated by colour from red (less important) to yellow (most important). In FA, relevant regions included; corpus callosum, left and right cingulum bundles, posterior limb of internal capsule, cerebral peduncle and post-thalamic radiation. In MD, RD and AD relevant regions in this case were very similar and included; caudate, medial frontal gyrus, parahippocampal gyrus and insula. Multi-slice views of these *consensus sensitivity maps* are shown in the Supplementary material.

Fig. 6 shows the best-fit function (rational-quadratic) of relevant anatomical region's average FA against actual age. This indicates a rapid acceleration in cerebral white matter maturation followed by a peaking age at around 21.8 years and finally a slow but consistent decrease in FA. Further details about rational-quadratic fits are explored in the Supplementary material. Table 4 shows several goodness-of-fit statistical measures used to estimate the validity of the rational-quadratic fit as compared to other polynomial fits. The rational-quadratic fit function had the best R-square value (0.453), indicating the function's ability to explain 45.3% of variance in the data. We propose that with a larger sample size it may be possible for this rational-quadratic function to give an even better fit (higher R-square value).

In RD, MD and AD average values from relevant anatomical regions in grey matter consistently increased with ageing indicating that grey matter tissue molecular diffusivity increases with ageing. Polynomial trajectories of these three DTI measurements are shown in the Supplementary material.

There was no interaction between gender and model prediction errors or residuals meaning that the model's ability to make accurate predictions was not influenced by the subjects' gender as shown in Table 2.

Discussion

To our knowledge, this is the first study to report predictions of individual subject's age using whole-brain DTI-derived scalar metrics. All four DTI measurement volumes (FA, MD, RD and AD) successfully predicted age with high *accuracy* as evaluated using various statistical measures for multivariate regression models. These results demonstrate that although brain maturation and healthy ageing effects may be subtle, DTI measurements contain sufficient information to detect these effects and predict individual subject's age accurately. Interestingly, our results show that it's possible to predict younger subjects (<30.5 years) more accurately (less actual vs predicted MAE and RMSE) than older subjects (>30.5). This can partly be explained by age related pathological changes in older subjects which are not necessarily present in younger subjects (Franke et al., 2010). There were no significant differences in prediction errors (actual vs predicted — MAE, RMSE) between male and female subjects. This indicates that the model's ability to make predictions was not influenced by any gender related anatomical differences. This corroborates previous evidence that there are no sex or gender related differences in cerebral white matter maturation and ageing (Inano et al., 2011; Virta et al.,

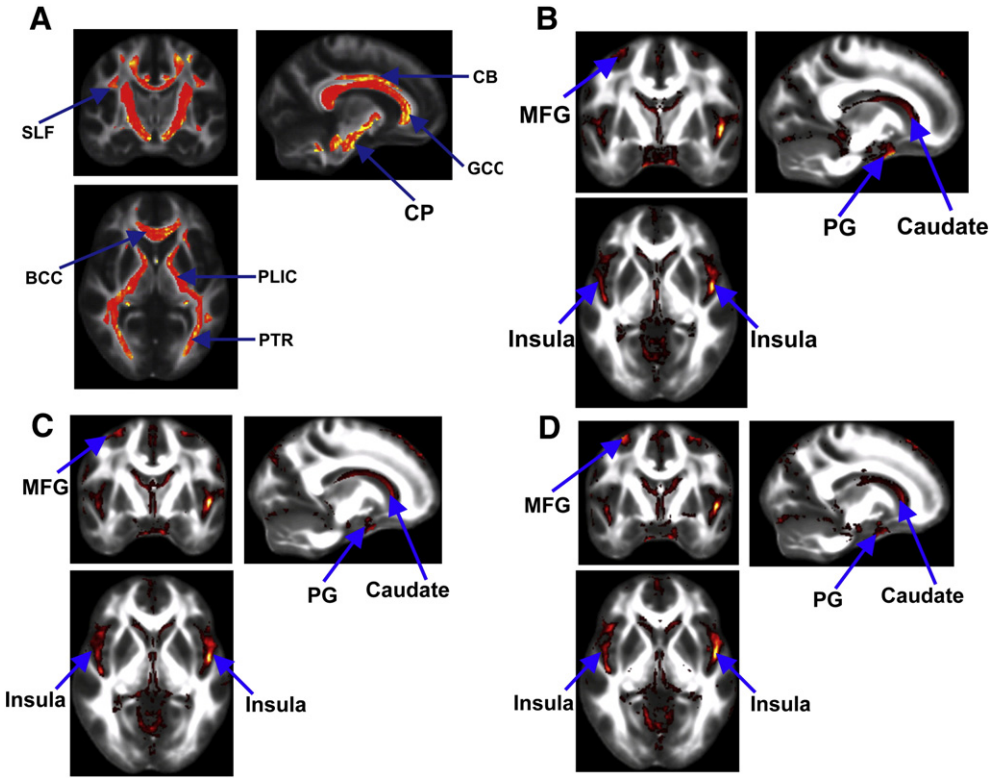

Fig. 5. LOOCV *consensus* sensitivity maps showing relevant anatomical regions selected in all four regression models. A) FA: BCC — body of corpus callosum, GCC — genu of corpus callosum, PLIC — posterior limb of internal capsule, PTR — posterior thalamic radiation (including optic radiation), CP — cerebral peduncle, SLF — superior longitudinal fasciculus. Anatomical regions were labelled using the John Hopkins University ICBM-DTI-81 white matter atlas (Mori et al., 2008). B) RD, C) MD, and D) AD. Relevant regions included; caudate, insula, medial frontal gyrus (MFG) and parahippocampal gyrus (PG). Multislice views are provided in the Supplementary material.

1999) although minimal sex differences have been reported in other studies (Abe et al., 2002; Hsu et al., 2008; Kochunov et al., 2012).

Image registration

Registration of DTI images into a common space without interfering with white matter tissue topology is not straightforward and somewhat remains an open research question (Mohammadi et al., 2012). In this study, we chose FNIRT image registration method (Smith et al., 2006) as it is reported to sufficiently align DTI images to a common template whilst keeping the white matter structure intact (Smith et al., 2006). However, since we executed FNIRT (Smith et al., 2006) as part of '*tbss_2_reg*' routine in FSL package, we avoided the subsequent step of 'skeletonization' of white matter tracts as we wanted to expose the model to both grey and white matter structures especially in MD, AD and RD. We note that there is no general consensus in the DTI research community as to which registration method is best. However, by using FNIRT (Smith et al., 2006), we report highly *accurate* age predictions indicating DTI's ability to detected ageing effects unrelated to any subtle misregistration errors that may occur. We also attempted to predict age using the image registration Jacobian volumes in FA which resulted into poor prediction accuracy (MAE = 13.92, RMSE = 17.65, R = 0.474, R^2 = 0.225). This demonstrates that our predictions were not driven by misregistration

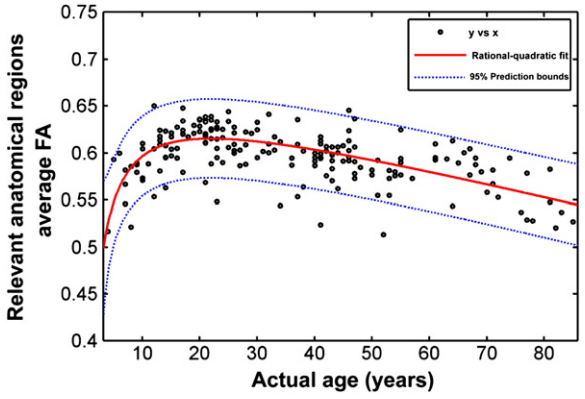

Fig. 6. A rational-quadratic fit of average FA calculated from 'relevant anatomical regions' and individual subject's actual age. Blue 'dashed' lines represent 95% prediction bounds. The function's turning point (maxima) was 21.8 years representing white matter cerebral maturation peak. Concurrent linear, quadratic and cubic fits in a single figure are reported in the Supplementary material.

Table 4
Table highlighting most relevant regions in each DTI measurement.

DTI measurement	Anatomical region	Cluster centroid (MNI coordinates)	Cluster size (voxels)
MD	Superior temporal gyrus	46, 18, −21	3329
	Superior frontal gyrus	23, 42, 32	2163
	Inferior frontal gyrus	−43, 27, −25	1569
	Caudate	13, 15, 0	1530
	Middle frontal gyrus	−25, 21, 39	861
AD	Superior temporal gyrus	−42, 21, −24	2303
	Lingual cerebellar	−2, −50, −25	2305
	Anterior cingulate	−9, 29, −9	852
	Middle frontal gyrus	28, 24, 37	901
RD	Superior temporal gyrus	45, 17, −19	4804
	Anterior cingulate	0, 20, −8	4451
	Postcentral gyrus	42, −19, 32	1300
	Middle frontal gyrus	27, 26, 38	702
FA	Superior cerebral peduncle	−6, −37, −22	4595
	Genu of corpus callosum	−13, 31, 1	1625
	Post-thalamic radiation	−35, −60, 6	921
	Body of corpus callosum	−11, −8, 33	614

errors. In another study, Ashburner (Ashburner, 2007), used RVR age predictions on T_1-weighted scans as a surrogate marker of an image registration algorithm's accuracy.

Relevant anatomical regions in FA

Cerebral white matter regions identified by the model as the most relevant for making accurate age predictions in FA have extensively been highlighted in other cerebral maturation and ageing studies. The corpus callosum (CC) is a major commissure connecting both cerebral hemispheres (Keshavan et al., 2002). In this study, CC (including its genu, splenium and body subdivisions) was particularly important in making age predictions with FA. Several studies have recently concluded that CC especially the genu is particularly vulnerable to age-related micro-structural changes (Hasan et al., 2009a, 2009b; Kochunov et al., 2007; Pfefferbaum et al., 2000; Salat et al., 2005a; Sullivan et al., 2001; Teipel et al., 2010).

The superior longitudinal fasciculus (SLF) is an association bundle connecting frontal lobe cortex to temporal, parietal and occipital lobe cortices (Jellison et al., 2004). Lebel and colleagues recently reported that FA in SLF increases with healthy development whilst reaching a plateau during the late teens or early twenties (Lebel et al., 2008). Other cerebral white matter regions notably relevant in making predictions in this study included; left and right cingulum bundles (CB), cerebral peduncle (CP) and posterior limbs of the internal capsule (PLIC). Pfefferbaum and colleagues reported decreased FA in anterior CB in older subjects (Pfefferbaum et al., 2005). This may explain the deterioration in cognitive function with ageing, which is repeatedly associated with the prefrontal cortices (Kochunov et al., 2012; Pfefferbaum et al., 2005; Raz, 2004). Hermoye and colleagues (Hermoye et al., 2006) reported the CP fibre bundles progressively thicken and anisotropy increases pointing to heavy myelination during maturation. Salat and colleagues reported that PLIC shows a significant age-related reduction in FA (Salat et al., 2005a, 2005b). Animal studies have also reported age-related white matter alterations in the SLF, CB and CC in rhesus monkeys (Makris et al., 2007; Salat et al., 2009).

Relevant anatomical regions in RD, MD and AD

The model's preference to select grey matter structures as the most relevant for making predictions in RD, MD and AD is unclear and contrary to our expectations. However, this is an encouraging finding given that previous studies have indicated the possibility of age-related water diffusivity changes in grey matter structures such as caudate (Hasan et al., 2007a), insula cortex (Foundas et al., 1998), parahippocampal gyrus (Burgmans et al., 2011) and superior temporal gyrus (Benedetti et al., 2006; Bhagat and Beaulieu, 2004; Lebel et al., 2008; Salat et al., 2009). Our findings confirm previous reports that there is a consistent increase in molecular diffusivity in grey matter tissue with healthy ageing (Bhagat and Beaulieu, 2004; Hasan, 2010; Pfefferbaum et al., 2010) although this theory is disputed by a few reports (Benedetti et al., 2006; Q. Wang et al., 2010).

Multivariate derived cerebral maturation and ageing trajectories

Linear and non-linear cerebral maturation and ageing trajectories in both grey and white matter have been reported in previous lifespan studies (Hasan, 2010; Hasan et al., 2007b, 2009a, 2009b) with converging evidence that majority of white matter structures *individually* follow non-linear trajectories (Hasan et al., 2007b; Lebel et al., 2008; Westlye et al., 2010). Kochunov et al. (2012) recently estimated *global* whole-brain age-related maturation and ageing trajectories by fitting FA measurements into a linear mixed effects model and reported a peaking age of 32.1 ± 5.9 years. Here though, we assumed that cerebral maturation and ageing are fairly a global process (whole-brain) with inter-regional multivariate interactions. We reported a FA peaking age of 21.8 years which substantiates previous reports that the whole brain white matter maturation trajectory peaks as early as the second decade of life (Imperati et al., 2011; Kochunov et al., 2012). Correspondingly, it has also been reported that overall performance on a number of cognitive tasks reaches its peak between (22–42 years) (Salthouse, 2009). MD, RD and AD in grey matter increased consistently with ageing which also corroborates previous reports that molecular diffusivity in grey matter increases with ageing (Hasan, 2010).

The benefits of a multivariate recursive feature elimination using sensitivity maps extracted from a radial-basis function driven model should be noted. First, a previous study (Ashburner, 2007) reported that a RVR model with a non-linear RBF kernel function is superior in predicting individual subject's age from T_1-weighted scans as compared to a linear kernel function. Second, Rasmussen and colleagues (Rasmussen et al., 2011) also report that RBF kernel function models are more superior as compared to linear kernel function models. Lastly, we also tried a recursive feature elimination process with a linear kernel function which resulted in poor performance (large mean absolute errors).

Limitations

Potential limitations of this study should be noted. First, samples were from a cross-sectional sample whilst maturation and ageing may be regarded as a longitudinal process (Kochunov et al., 2012) and further studies should be carried out using a longitudinal design to confirm these findings. However, challenges of performing longitudinal studies such as time, subject withdrawal, subject migration and expense should also be noted (Hedden and Gabrieli, 2004). Second, the cohort's age distribution was slightly skewed between (10–30 years, 44%). There were more males than females (110 males vs 78 males) although when stratified at 5 year interval (see the Supplementary materials) this difference was not statistically significant (unpaired two-tailed *t*-test $p = 0.2231$).

Conclusions

In conclusion, we have reported highly *accurate* multivariate machine learning predictions of individual subject's age using four DTI-derived scalar metrics. Anatomical regions relevant in making highly *accurate* predictions indicated FA possibly peaks in the second decade and molecular diffusivity in grey matter structures increases consistently with ageing. We note that work is ongoing in our group to develop an 'ensemble regression model' which combines features from FA, MD, RD and AD to further improve prediction *accuracies* (less MAE, RMSE and high R-square). These results demonstrate that DTI measurements sufficiently encode healthy cerebral maturation and ageing microstructural changes across lifespan. Second and perhaps most remarkable, these data confirm previous reports that cerebral maturation and ageing patterns follow a non-linear trajectory across human lifespan. However, from a neuropsychiatric perspective, these results may contribute to distinguishing cerebral changes that may occur due to healthy maturation or ageing, and those due to developmental or neuropsychiatric disorders.

Acknowledgments

Data used in this study were obtained from the International Neuroimaging Data Sharing Initiative (INDI) online database (http://fcon_1000.projects.nitrc.org/indi/pro/nki.html) as part of the original Nathan Kline Institute/Rockland sample. We acknowledge the entire INDI team involved in data acquisition and management especially Dr. Maarten Mennes for answering various questions regarding the

data. The INDI team was not involved in data analysis or report preparation.

Conflict of interest

This work was funded by NIH-NINDS R01-NS052505-04 and Dunn Research Foundation to K.M.H, NIMH RO1085667 and Pat Rutherford, Jr. Endowed Chair in Psychiatry (UT Medical School) to J.C.S. J.C.S has participated in research funded by Forest, Merck, BMS, GSK. He has been a speaker for Pfizer and Abott.

Appendix A. Relevance vector regression

We recall the input-target pair $\{X_i,t_i\}_{i=1}^{N}$, which is later generalised into a linear model $t_i = \sum_{i=1}^{N} \omega_i K(x,x_i) + c + \varepsilon_i$. In order to estimate the weighting factors $W = (\omega_1, \omega_2, \ldots \omega_N)^T$, RVR adopts a Bayesian framework:

$$\text{Posterior distribution} = \frac{\text{likelihood} \times \text{prior}}{\text{marginal distribution}(\text{normalization factor})}. \tag{A1}$$

As a result, the likelihood of the data is represented as;

$$p\left(t|W,\sigma^2\right) = \left(2\pi\sigma^2\right)^{-N/2} \exp\left\{-\frac{1}{2\sigma^2}||t-\Phi W||^2\right\} \tag{A2}$$

where, $t = (t_1 \ldots t_N)^T$, Φ is an $N \times (N+1)$ design matrix defined as $\Phi = [\phi(x_1), \phi(x_2), \ldots, \phi(x_N)]^T$ and $\phi(x_n) = [1, K(x_n,x_1), K(x_n,x_2), \ldots, K(x_n,x_N)]$. We recall that $K(x,x)$ is a kernel mapping procedure (e.g. linear or radial basis function). The above likelihood is similar to the standard least-square estimate and suffers from overfitting — meaning that the model is not able to generalise well from novel testing examples (Tipping, 2001). To avoid overfitting a 'regularization' approach is adopted by introducing a zero-mean Gaussian prior distribution of the parameters defined as;

$$p\left(W|\alpha\right) = \prod_{n=0}^{N} N\left(\omega_n|0,\alpha_n^{-1}\right) \tag{A3}$$

α is a vector of $N \times 1$ hyperparameters and each weighting parameter (ω_n) is paired with corresponding hyperparameters. The process of defining hyperparameter priors (hyper-priors) and noise variance σ^2 is described in greater length elsewhere (Bishop, 2006; Tipping, 2001). The Bayesian formulation introduced in (A1) is now completed using the likelihood (A2) and prior (A3) as:

$$p\left(W|t,\alpha,\sigma^2\right) = \frac{p\left(t|W,\sigma^2\right)p(W|\alpha)}{p(t|\alpha,\sigma^2)}. \tag{A4}$$

The posterior distribution (left hand) follows a Gaussian distribution with mean μ and covariance Σ.

$$\begin{aligned} &p\left(W|t,\alpha,\sigma^2\right) = N(\mu,\Sigma) \\ &\mu = \sigma^{-2}\Sigma\Phi^T t \\ &\Sigma = \left(\sigma^{-2}\Phi^T\Phi + A\right)^{-1} \\ &A = diag(\alpha_0,\alpha_1,\ldots\alpha_N) \end{aligned} \tag{A5}$$

A is a diagonal matrix representing the inverse of the noise for each weight. A solution is obtained by maximising the marginal likelihood (denominator in A1 and A4) using the type-II maximum likelihood algorithm and further details about this process are given elsewhere (Bishop, 2006; Tipping, 2001).

Most importantly, during this process some of the estimated hyperparameters (α) tend towards infinity, which suggests a small prior variance and corresponding weighting factors constrained to zero. These weighting factors are 'pruned out' (weighting values set to zero) using the automatic relevance determination method (Mackay, 1994). This process yields a sparse model — meaning only a 'small fraction' of the training examples have non-zero weights (Tipping, 2001). Training examples with non-zero weights are known as 'relevance vectors'. Finally, RVR predictions on test data (not used during training) are defined as

$$t_{new} = \sum_{n=0}^{N} \mu_n \phi_n \tag{A6}$$

μ represents the weights estimated above, and ϕ represents training examples from the $N \times (N+1)$ design matrix introduced earlier (A2).

Appendix B. Sensitivity maps

Linear sensitivity maps

Sensitivity maps contain individual voxel weighted values signifying a voxel's relevance to a predictive model. Linear RVR model sensitivity maps can be extracted directly from model input data and corresponding model derived weighting factors as follows

$$S = \sum_i \alpha_i x_{i,j} \tag{B1}$$

where $x_{i,j}$ represents the jth voxel of training example i and α stands for a model weighting factor.

Non-linear sensitivity maps

Several reports have previously proposed extraction of sensitivity maps or voxel weight maps from non-linear kernel models (Kjems et al., 2002; LaConte et al., 2005; Rasmussen et al., 2011). First, the kernel matrix (K_x) is represented as $K(x_i,x) = \exp\left(-||x_i-x||_q^2\right)$, x_i and x stand for training example data and q stands for the *kernel width parameter*. The sensitivity values of every voxel can be extracted by calculating the derivative of the kernel matrix:

$$\begin{aligned} \frac{\partial \alpha^T K_x}{\partial x_j} &= \frac{\partial \sum_i \alpha_i \exp\left(-\frac{||x_i-x||^2}{q}\right)}{\partial x_j} \\ &= \sum_i \alpha_i 2 \frac{\left(x_{i,j}-x_j\right)}{q} \exp\left(-\frac{||x_i-x||^2}{q}\right). \end{aligned} \tag{B2}$$

The output is an individual voxel weighting value indicating the voxel's importance to the predictive model (Kjems et al., 2002; LaConte et al., 2005; Rasmussen et al., 2011).

Appendix C. Supplementary data

Supplementary data to this article can be found online at http://dx.doi.org/10.1016/j.neuroimage.2013.02.055.

References

Abe, O., Aoki, S., Hayashi, N., Yamada, H., Kunimatsu, A., Mori, H., Yoshikawa, T., Okubo, T., Ohtomo, K., 2002. Normal aging in the central nervous system: quantitative MR diffusion-tensor analysis. Neurobiol. Aging 23, 433–441.

Abe, O., Yamasue, H., Aoki, S., Suga, M., Yamada, H., Kasai, K., Masutani, Y., Kato, N., Kato, N., Ohtomo, K., 2008. Aging in the CNS: comparison of gray/white matter volume and diffusion tensor data. Neurobiol. Aging 29, 102–116.

Ashburner, J., 2007. A fast diffeomorphic image registration algorithm. NeuroImage 38, 95–113.

Barnea-Goraly, N., Menon, V., Eckert, M., Tamm, L., Bammer, R., Karchemskiy, A., Dant, C.C., Reiss, A.L., 2005. White matter development during childhood and adolescence: a cross-sectional diffusion tensor imaging study. Cereb. Cortex 15, 1848–1854.

Basser, P.J., Pierpaoli, C., 1996. Microstructural and physiological features of tissues elucidated by quantitative-diffusion-tensor MRI. J. Magn. Reson. 213, 560–570.

Benedetti, B., Charil, A., Rovaris, M., Judica, E., Valsasina, P., Sormani, M.P., Filippi, M., 2006. Influence of aging on brain gray and white matter changes assessed by conventional, MT, and DT MRI. Neurology 66, 535–539. http://dx.doi.org/10.1212/01.wnl.0000198510.73363.c6.

Benes, F.M., Turtle, M., Khan, Y., Farol, P., 1994. Myelination of a key relay zone in the hippocampal formation occurs in the human brain during childhood, adolescence, and adulthood. Arch. Gen. Psychiatry 51, 477–484.

Bhagat, Y.A., Beaulieu, C., 2004. Diffusion anisotropy in subcortical white matter and cortical gray matter: changes with aging and the role of CSF-suppression. J. Magn. Reson. Imaging 20, 216–227.

Bishop, C., 2006. Pattern Recognition and Machine Learning. Springer, New York.

Brown, T., Kuperman, J.M., Chung, Y., Erhart, M., McCabe, C., Hagler Jr., D.J., Venkatraman, V.K., Akshoomoff, N., Amaral, D., Bloss, C.S., Casey, B.J., Chang, L., Ernst, T.M., Frazier, J.A., Gruen, J.R., Kaufmann, W.E., Kenet, T., Kennedy, D.N., Murray, S.S., Sowell, E.R., Jernigan, T.L., Dale, A.M., 2012. Neuroanatomical assessment of biological maturity. Curr. Biol. 22, 1693–1698.

Burgmans, S., van Boxtel, M.P.J., van den Berg, K.E.M., Gronenschild, E.H.B.M., Jacobs, H.I.L., Jolles, J., Uylings, H.B.M., 2011. The posterior parahippocampal gyrus is preferentially affected in age-related memory decline. Neurobiol. Aging 32, 1572–1578.

Camara, E., Bodammer, N., Rodriguez-Fornells, A., Tempelmann, C., 2007. Age-related water diffusion changes in human brain: a voxel-based approach. NeuroImage 34, 1588–1599.

Cascio, C.J., Gerig, G., Piven, J., 2007. Diffusion tensor imaging: application to the study of the developing brain. J. Am. Acad. Child Adolesc. Psychiatry 46, 213–223.

Cherubini, A., PÃ©ran, P., Caltagirone, C., Sabatini, U., Spalletta, G., 2009. Aging of subcortical nuclei: microstructural, mineralization and atrophy modifications measured in vivo using MRI. NeuroImage 48, 29–36.

Chiang, M.C., Barysheva, M., Shattuck, D.W., Lee, A.D., Madsen, S.K., Avedissian, C., Klunder, A.D., Toga, A.W., McMahon, K.L., De Zubicaray, G.I., 2009. Genetics of brain fiber architecture and intellectual performance. J. Neurosci. 29, 2212–2224.

Dosenbach, N.U.F., Nardos, B., Cohen, A.L., Fair, D.A., Power, J.D., Church, J.A., Nelson, S.M., Wig, G.S., Vogel, A.C., Lessov-Schlaggar, C.N., Barnes, K.A., Dubis, J.W., Feczko, E., Coalson, R.S., Pruett Jr., J.R., Barch, D.M., Petersen, S.E., Schlaggar, B.L., 2010. Prediction of individual brain maturity using fMRI. Science 329, 1358–1361.

Eluvathingal, T.J., Hasan, K.M., Kramer, L., Fletcher, J.M., Ewing-Cobbs, L., 2007. Quantitative diffusion tensor tractography of association and projection fibers in normally developing children and adolescents. Cereb. Cortex 17, 2760–2768.

Formisano, E., De Martino, F., Valente, G., 2008. Multivariate analysis of fMRI time series: classification and regression of brain responses using machine learning. Magn. Reson. Imaging 26, 921–934 (Proceedings of the International School on Magnetic Resonance and Brain Function Proceedings of the International School on Magnetic Resonance and Brain Function).

Foundas, A., Zipin, D., Browning, C., 1998. Age-related changes of the insular cortex and lateral ventricles: conventional MRI volumetric measures. J. Neuroimaging 8, 216–221.

Franke, K., Ziegler, G., Kloppel, S., Gaser, C., 2010. Estimating the age of healthy subjects from T1-weighted MRI scans using kernel methods: exploring the influence of various parameters. NeuroImage 50, 883–892.

Grieve, S.M., Williams, L.M., Paul, R.H., Clark, C.R., Gordon, E., 2007. Cognitive aging, executive function, and fractional anisotropy: a diffusion tensor MR imaging study. AJNR Am. J. Neuroradiol. 28, 226–235.

Gunning-Dixon, F.M., Brickman, A.M., Cheng, J.C., Alexopoulos, G.S., 2009. Aging of cerebral white matter: a review of MRI findings. Int. J. Geriatr. Psychiatry 24, 109–117.

Guyon, I., Elisseeff, A., 2003. An introduction to variable and feature selection. J. Mach. Learn. Res. 3, 1157–1182.

Guyon, I., Weston, J., Barnhill, S., Vapnik, V., 2002. Gene selection for cancer classification using support vector machines. Mach. Learn. 46, 389–422.

Hasan, K.M., 2010. Simple linear regression model is misleading when used to analyze quantitative diffusion tensor imaging data that include young and old adults. AJNR Am. J. Neuroradiol. 31, E80.

Hasan, K.M., Frye, R.E., 2011. Diffusion tensor-based regional gray matter tissue segmentation using the international consortium for brain mapping atlases. Hum. Brain Mapp. 32, 107–117.

Hasan, K.M., Halphen, C., Boska, M.D., Narayana, P.A., 2007a. Diffusion tensor metrics, T2 relaxation, and volumetry of the naturally aging human caudate nuclei in healthy young and middle-aged adults: possible implications for the neurobiology of human brain aging and disease. Magn. Reson. Med. 59, 7–13.

Hasan, K.M., Sankar, A., Halphen, C., Kramer, L.A., Brandt, M.E., Juranek, J., Cirino, P.T., Fletcher, J.M., Papanicolaou, A.C., Ewing-Cobbs, L., 2007b. Development and organization of the human brain tissue compartments across the lifespan using diffusion tensor imaging. Neuroreport 18, 1735.

Hasan, K.M., Ewing-Cobbs, L., Kramer, L.A., Fletcher, J.M., Narayana, P.A., 2008. Diffusion tensor quantification of the macrostructure and microstructure of human midsagittal corpus callosum across the lifespan. NMR Biomed. 21, 1094–1101.

Hasan, K.M., Halphen, C., Kamali, A., Nelson, F.M., Wolinsky, J.S., Narayana, P.A., 2009a. Caudate nuclei volume, diffusion tensor metrics, and T2 relaxation in healthy adults and relapsing–remitting multiple sclerosis patients: implications for understanding gray matter degeneration. J. Magn. Reson. Imaging 29, 70–77.

Hasan, K.M., Kamali, A., Iftikhar, A., Kramer, L.A., Papanicolaou, A.C., Fletcher, J.M., Ewing-cobbs, L., 2009b. Diffusion tensor tractography quantification of the human corpus callosum fiber pathways across the lifespan. Brain Res. 1249, 91–100.

Haynes, J.D., Rees, G., 2006. Decoding mental states from brain activity in humans. Nat. Rev. Neurosci. 7, 523–534.

Head, D., Buckner, R.L., Shimony, J.S., Williams, L.E., Akbudak, E., Conturo, T.E., McAvoy, M., Morris, J.C., Snyder, A.Z., 2004. Differential vulnerability of anterior white matter in nondemented aging with minimal acceleration in dementia of the Alzheimer type: evidence from diffusion tensor imaging. Cereb. Cortex 14, 410–423.

Hedden, T., Gabrieli, J.D.E., 2004. Insights into the ageing mind: a view from cognitive neuroscience. 5, 87–96.

Hermoye, L., Saint-Martin, C., Cosnard, G., Lee, S.-K., Kim, J., Nassogne, M.-C., Menten, R., Clapuyt, P., Donohue, P.K., Hua, K., Wakana, S., Jiang, H., van Zijl, P.C.M., Mori, S., 2006. Pediatric diffusion tensor imaging: normal database and observation of the white matter maturation in early childhood. NeuroImage 29, 493–504.

Hsu, J.-L., Leemans, A., Bai, C.-H., Lee, C.-H., Tsai, Y.-F., Chiu, H.-C., Chen, W.-H., 2008. Gender differences and age-related white matter changes of the human brain: a diffusion tensor imaging study. NeuroImage 39, 566–577.

Hsu, J.-L., Van Hecke, W., Bai, C.-H., Lee, C.-H., Tsai, Y.-F., Chiu, H.-C., Jaw, F.-S., Hsu, C.-Y., Leu, J.-G., Chen, W.-H., Leemans, A., 2010. Microstructural white matter changes in normal aging: a diffusion tensor imaging study with higher-order polynomial regression models. NeuroImage 49, 32–43.

Huttenlocher, P.R., 1979. Synaptic density in human frontal cortex — developmental changes and effects of aging. Brain Res. 163, 195–205.

Huttenlocher, P.R., de Courten, C., 1987. The development of synapses in striate cortex of man. Hum. Neurobiol. 6, 1–9.

Imperati, D., Colcombe, S., Kelly, C., Di Martino, A., Zhou, J., Castellanos, F.X., Milham, M.P., 2011. Differential development of human brain white matter tracts. PLoS One 6, e23437 (EP).

Inano, S., Takao, H., Hayashi, N., Abe, O., Ohtomo, K., 2011. Effects of age and gender on white matter integrity. Am. J. Neuroradiol. 32, 2103–2109.

Jellison, B.J., Field, A.S., Medow, J., Lazar, M., Salamat, M.S., Alexander, A.L., 2004. Diffusion tensor imaging of cerebral white matter: a pictorial review of physics, fiber tract anatomy, and tumor imaging patterns. Am. J. Neuroradiol. 25, 356–369.

Johansen-Berg, H., Behrens, T., 2009. Diffusion MRI — From Quantitative Measurement to In-vivo Neuroanatomy. Elsevier, London.

Johnston, B., Mwangi, B., Matthews, K., Coghill, D., Steele, J., 2012. Predictive classification of individual magnetic resonance imaging scans from children and adolescents. European Child & Adolescent Psychiatry. Springer, Berlin/Heidelberg, pp. 1–12.

Kanda, T., Tsukagoshi, H., Oda, M., Miyamoto, K., Tanabe, H., 1991. Morphological changes in unmyelinated nerve fibres in the sural nerve with age. Brain 114 (Pt 1B), 585–599.

Kennedy, K.M., Raz, N., 2009. Aging white matter and cognition: differential effects of regional variations in diffusion properties on memory, executive functions, and speed. Neuropsychologia 47, 916–927.

Keshavan, M.S., Diwadkar, V.A., DeBellis, M., Dick, E., Kotwal, R., Rosenberg, D.R., Sweeney, J.A., Minshew, N., Pettegrew, J.W., 2002. Development of the corpus callosum in childhood, adolescence and early adulthood. Life Sci. 70, 1909–1922.

Kjems, U., Hansen, L.K., Anderson, J., Frutiger, S., Muley, S., Sidtis, J., Rottenberg, D., Strother, S., 2002. The quantitative evaluation of functional neuroimaging experiments: mutual information learning curves. NeuroImage 15, 772–786.

Klingberg, T., Vaidya, C.J., Gabrieli, J.D.E., Moseley, M.E., Hedehus, M., 1999. Myelination and organization of the frontal white matter in children: a diffusion tensor MRI study. Neuroreport 10, 2817–2821.

Kochunov, P., Thompson, P.M., Lancaster, J.L., Bartzokis, G., Smith, S., Coyle, T., Royall, D.R., Laird, A., Fox, P.T., 2007. Relationship between white matter fractional anisotropy and other indices of cerebral health in normal aging: tract-based spatial statistics study of aging. NeuroImage 35, 478–487.

Kochunov, P., Glahn, D.C., Lancaster, J.L., Winkler, A.M., Smith, S., Thompson, P.M., Almasy, L., Duggirala, R., Fox, P.T., Blangero, J., 2010. Genetics of microstructure of cerebral white matter using diffusion tensor imaging. NeuroImage 53, 1109–1116.

Kochunov, P., Williamson, D.E., Lancaster, J., Fox, P., Cornell, J., Blangero, J., Glahn, D.C., 2012. Fractional anisotropy of water diffusion in cerebral white matter across the lifespan. Neurobiol. Aging 33, 9–20.

Kohannim, O., Jahanshad, N., Braskie, M.N., Stein, J.L., Chiang, M.-C., Reese, A.H., Hibar, D.P., Toga, A.W., McMahon, K.L., de Zubicaray, G.I., Medland, S.E., Montgomery, G.W., Martin, N.G., Wright, M.J., Thompson, P.M., 2012. Predicting White Matter Integrity From Multiple Common Genetic Variants.

Kumar, R., Nguyen, H.D., Macey, P.M., Woo, M.A., Harper, R.M., 2012. Regional brain axial and radial diffusivity changes during development. J. Neurosci. Res. 90, 346–355.

Lachenbruch, P., Mickey, M., 1968. Estimation of error rates in discriminant analysis. Technometrics 10, 1–10.

LaConte, S., Strother, S., Cherkassky, V., Anderson, J., Hu, X., 2005. Support vector machines for temporal classification of block design fMRI data. NeuroImage 26, 317.

Lebel, C., Walker, L., Leemans, A., Phillips, L., Beaulieu, C., 2008. Microstructural maturation of the human brain from childhood to adulthood. NeuroImage 40, 1044–1055.

Lebel, C., Gee, M., Camicioli, R., Wieler, M., Martin, W., Beaulieu, C., 2012. Diffusion tensor imaging of white matter tract evolution over the lifespan. NeuroImage 60, 340–352.

Liu, Y., Aeby, A., Baleriaux, D., David, P., Absil, J., De Maertelaer, V., Van Bogaert, P., Avni, F., Metens, T., 2012. White matter abnormalities are related to microstructural changes in preterm neonates at term-equivalent age: a diffusion tensor imaging and probabilistic tractography study. AJNR Am. J. Neuroradiol. 33, 839–845.
Mackay, D., 1994. Bayesian methods for backpropagation networks. Models of Neural Networks III.Springer, New York.
Makris, N., Papadimitriou, G.M., van der Kouwe, A., Kennedy, D.N., Hodge, S.M., Dale, A.M., Benner, T., Wald, L.L., Wu, O., Tuch, D.S., 2007. Frontal connections and cognitive changes in normal aging rhesus monkeys: a DTI study. Neurobiol. Aging 28, 1556–1567.
Malykhin, N., Vahidy, S., Michielse, S., Coupland, N., Camicioli, R., Seres, P., Carter, R., 2011. Structural organization of the prefrontal white matter pathways in the adult and aging brain measured by diffusion tensor imaging. Brain Structure and Function, vol. 216. no. 4. Springer, Berlin/Heidelberg, pp. 417–431.
Mayer, D., Butler, D., 1993. Statistical validation. Ecol. Model. 68, 21–32.
Mohammadi, S., Keller, S.S., Glauche, V., Kugel, H., Jansen, A., Hutton, C., FlÃ¶el, A., Deppe, M., 2012. The influence of spatial registration on detection of cerebral asymmetries using voxel-based statistics of fractional anisotropy images and TBSS. PLoS One 7, e36851 (EP).
Mori, S., Oishi, K., Jiang, H., Jiang, L., Li, X., Akhter, K., Hua, K., Faria, A.V., Mahmood, A., Woods, R., Toga, A.W., Pike, G.B., Neto, P.R., Evans, A., Zhang, J., Huang, H., Miller, M.I., Van Zijl, P., Mazziotta, J., 2008. Stereotaxic white matter atlas based on diffusion tensor imaging in an ICBM template. Neuroimage 40 (2), 570–582.
Moseley, M., 2002. Diffusion tensor imaging and aging — a review. NMR Biomed. 15, 553–560.
Mwangi, B., Matthews, K., Steele, J.D., 2012a. Prediction of illness severity in patients with major depression using structural MR brain scans. J. Magn. Reson. Imaging 35, 64–71.
Mwangi, B., Ebmeier, K.P., Matthews, K., Douglas Steele, J., 2012b. Multi-centre diagnostic classification of individual structural neuroimaging scans from patients with major depressive disorder. Brain 135, 1508–1521.
Ota, M., Obata, T., Akine, Y., Ito, H., Ikehira, H., Asada, T., Suhara, T., 2006. Age-related degeneration of corpus callosum measured with diffusion tensor imaging. NeuroImage 31, 1445–1452.
Penke, L., Maniega, S.M., Murray, C., Gow, A.J., HernÃ¡ndez, M.C.V., Clayden, J.D., Starr, J.M., Wardlaw, J.M., Bastin, M.E., Deary, I.J., 2010. A general factor of brain white matter integrity predicts information processing speed in healthy older people. J. Neurosci. 30, 7569–7574.
Pfefferbaum, A., Sullivan, E.V., 2003. Increased brain white matter diffusivity in normal adult aging: relationship to anisotropy and partial voluming. Magn. Reson. Med. 49, 953–961.
Pfefferbaum, A., Sullivan, E.V., Hedehus, M., Lim, K.O., Adalsteinsson, E., Moseley, M., 2000. Age-related decline in brain white matter anisotropy measured with spatially corrected echo-planar diffusion tensor imaging. Magn. Reson. Med. 44, 259–268.
Pfefferbaum, A., Adalsteinsson, E., Sullivan, E.V., 2005. Frontal circuitry degradation marks healthy adult aging: evidence from diffusion tensor imaging. NeuroImage 26, 891–899.
Pfefferbaum, A., Adalsteinsson, E., Rohlfing, T., Sullivan, E.V., 2010. Diffusion tensor imaging of deep gray matter brain structures: effects of age and iron concentration. Neurobiol. Aging 31, 482–493.
Rasmussen, P., Madsen, K., Lund, T., Hansen, L., 2011. Visualization of nonlinear kernel models in neuroimaging by sensitivity maps. NeuroImage 55, 1120–1131.
Raz, N., 2004. The aging brain observed in vivo: differential changes and their modifiers. In: Cabeza, R., et al. (Ed.), Cognitive Neuroscience of Aging: Linking Cognitive and Cerebral Aging. Oxford University Press, New York, pp. 17–55.
Salat, D.H., Tuch, D.S., Greve, D.N., van der Kouwe, A.J.W., Hevelone, N.D., Zaleta, A.K., Rosen, B.R., Fischl, B., Corkin, S., Rosas, H.D., Dale, A.M., 2005a. Age-related alterations in white matter microstructure measured by diffusion tensor imaging. Neurobiol. Aging 26, 1215–1227.
Salat, D.H., Tuch, D.S., Hevelone, N.D., Fischl, B., Corkin, S., Rosas, H.D., Dale, A.M., 2005b. Age-related changes in prefrontal white matter measured by diffusion tensor imaging. Ann. N. Y. Acad. Sci. 1064, 37–49.
Salat, D., Lee, S., Yu, P., Setty, B., Rosas, H., Grant, P.E., 2009. DTI in development and aging. In: Johansen-Berg, H., Behrens, T. (Eds.), Diffusion MRI: From Quantitative Measurement to In vivo Neuroanatomy. Academic Press, London, pp. 226–227.
Salthouse, T.A., 2009. When does age-related cognitive decline begin? Neurobiol. Aging 30, 507–514.
Schmithorst, V.J., Wilke, M., Dardzinski, B.J., Holland, S.K., 2002. Correlation of white matter diffusivity and anisotropy with age during childhood and adolescence: a cross-sectional diffusion-tensor MR imaging study. Radiology 222, 212–218.
Smith, S.M., 2002. Fast robust automated brain extraction. Hum. Brain Mapp. 17, 143–155.
Smith, S.M., Jenkinson, M., Johansen-Berg, H., Rueckert, D., Nichols, T.E., Mackay, C.E., Watkins, K.E., Ciccarelli, O., Cader, M.Z., Matthews, P.M., Behrens, T.E.J., 2006. Tract-based spatial statistics: voxelwise analysis of multi-subject diffusion data. NeuroImage 31, 1487–1505.
Smola, A.J., Scholkopf, B., 2004. A tutorial on support vector regression. Stat. Comput. 14, 199–222.
Song, S.-K., Sun, S.-W., Ramsbottom, M.J., Chang, C., Russell, J., Cross, A.H., 2002. Dysmyelination revealed through MRI as increased radial (but unchanged axial) diffusion of water. NeuroImage 17, 1429–1436.
Song, S.-K., Sun, S.-W., Ju, W.-K., Lin, S.-J., Cross, A.H., Neufeld, A.H., 2003. Diffusion tensor imaging detects and differentiates axon and myelin degeneration in mouse optic nerve after retinal ischemia. NeuroImage 20, 1714–1722.
Stadlbauer, A., Salomonowitz, E., Strunk, G., Hammen, T., Ganslandt, O., 2008a. Age-related degradation in the central nervous system: assessment with diffusion-tensor imaging and quantitative fiber tracking. Radiology 247, 179–188.
Stadlbauer, A., Salomonowitz, E., Strunk, G., Hammen, T., Ganslandt, O., 2008b. Quantitative diffusion tensor fiber tracking of age-related changes in the limbic system. European Radiology, vol. 18. no. 1. Springer, Berlin/Heidelberg, pp. 130–137.
Stonnington, C.M., Chu, C., Kloppel, S., Jack Jr., C.R., Ashburner, J., Frackowiak, R.S.J., 2010. Predicting clinical scores from magnetic resonance scans in Alzheimer's disease. NeuroImage 51, 1405–1413.
Sullivan, E.V., Pfefferbaum, A., 2006. Diffusion tensor imaging and aging. Neurosci. Biobehav. Rev 30, 749–761 Methodological and Conceptual Advances in the Study of Brain-Behavior Dynamics: A Multivariate Lifespan Perspective.
Sullivan, E.V., Adalsteinsson, E., Hedehus, M., Ju, C., Moseley, M., Lim, K.O., Pfefferbaum, A., 2001. Equivalent disruption of regional white matter microstructure in ageing healthy men and women. Proceedings of the Neuroreport, pp. 99–104.
Teipel, S.J., Meindl, T., Wagner, M., Stieltjes, B., Reuter, S., Hauenstein, K.-H., Filippi, M., Ernemann, U., Reiser, M.F., Hampel, H., 2010. Longitudinal changes in fiber tract integrity in healthy aging and mild cognitive impairment: a DTI follow-up study. J. Alzheimer's Dis. 22, 507–522.
Tipping, M., 2001. Sparse Bayesian learning and the relevance vector machine. J. Mach. Learn. Res. 1, 211–244.
Virta, A., Barnett, A., Pierpaoli, C., 1999. Visualizing and characterizing white matter fiber structure and architecture in the human pyramidal tract using diffusion tensor MRI. Magn. Reson. Imaging 17, 1121–1133.
Wang, Q., Xu, X., Zhang, M., 2010a. Normal aging in the basal ganglia evaluated by eigenvalues of diffusion tensor imaging. AJNR Am. J. Neuroradiol. 31, 516–520.
Wang, Y., Fan, Y., Bhatt, P., Davatzikos, C., 2010b. High-dimensional pattern regression using machine learning: from medical images to continuous clinical variables. NeuroImage 50, 1519–1535.
Westlye, L.T., Walhovd, K.B., Dale, A.M., Bjonerud, A., Due-Tonnessen, P., Engvig, A., Grydeland, H.K., Tamnes, C.K., Ostby, Y., Fjell, A.M., 2010. Life-Span changes of the human brain white matter: diffusion tensor imaging (DTI) and volumetry. Cereb. Cortex 20, 2055–2068. http://dx.doi.org/10.1093/cercor/bhp280.
Whitcher, B., Wisco, J.J., Hadjikhani, N., Tuch, D.S., 2007. Statistical group comparison of diffusion tensors via multivariate hypothesis testing. Magn. Reson. Med. 57, 1065–1074.
Ziegler, G., Dahnke, R., Gaser, C., 2012. Models of the aging brain structure and individual decline. Front. Neuroinform. 6, 3.